Science and Technology Infusion Climate Bulletin
NOAA's National Weather Service
43rd NOAA Annual Climate Diagnostics and Prediction Workshop
Santa Barbara, CA, 23-25 October 2018

Overview of the 2017-18 La Niña and El Niño Watch in Mid-2018

Michelle L'Heureux
Climate Prediction Center, NOAA/NWS/NCEP

1. ENSO evolution and forecasts during 2017-18

A second-year, weak-to-moderate La Niña developed in the fall of 2017 and lasted through early spring of 2018. This La Niña followed a period of ENSO-neutral conditions during the first half of 2017. From January to May 2017, many model forecasts of the Niño-3.4 region of sea surface temperatures were predicting El Niño to occur during the latter part of 2017. While not alone in these predictions, the 100-member spread of the American Multi-Model Ensemble (NMME) lay outside of the observed evolution, in which instead of a developing El Niño, the tropical Pacific instead went into a La Niña in September-November of 2017 (as indicated by the Oceanic Niño Index value of -0.7°C). The ensemble mean predictions of the Niño-3.4 index from the NMME are indicated by the grey lines in Fig. 1. However, because these forecasts for El Niño during late 2017 were initialized early in the year and through the spring prediction barrier, a time of lower model skill, the CPC/IRI ENSO team never issued an El Niño Watch despite probabilities for El Niño that were elevated (well in excess of 50% chance in the models).

Because nearly all members from NMME were too warm for targets in mid-to-late 2017, verification using Ranked Probability Skill Scores (RPSS) were strongly negative for almost all forecast leads (orange lines in Fig. 2). The CPC official forecast assigned probabilities for El Nino that were greater than climatology, but they were much less bullish than the objective model guidance, so RPSS scores were not as negative as for NMME (green lines in Fig. 2).

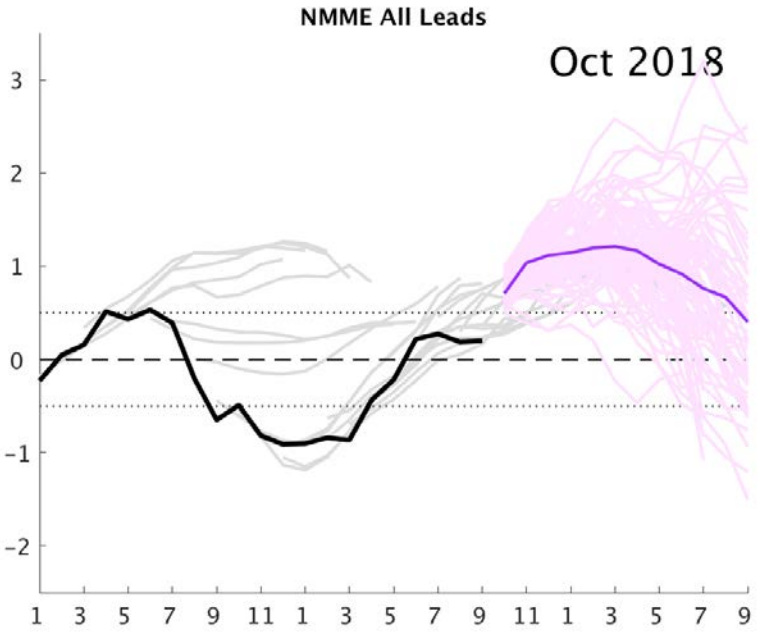

Fig. 1 Observed monthly Niño-3.4 index values (black line) from daily OISST (Reynolds *et al.* 2007) and once monthly forecasts of Niño-3.4 from the North American Multi-Model (NMME) from January 2017 through October 2018 (grey lines showing ensemble means). Departures are formed by removing monthly means during 1982-2010.

Many dynamical and statistical models did not catch onto the possible La Niña of 2017-18 until the observed Niño-3.4 index values dropped to thresholds consistent with La Niña (-0.5°C in ERSSTv5 data (Huang *et al.* 2017) in September 2017). It wasn't until early September initializations of the NMME that the ensemble mean forecasted La Niña to occur and persist through the 2017-18 winter. At this point, both CPC official forecasts and model predictions consistently favored La Niña, and RPSS became positive for very short lead times (Fig. 2, top row). A La Niña Watch was issued for the first time in early September 2017 and a La Niña Advisory was issued in early November 2017 as the onset of La Niña became apparent in both oceanic and atmospheric anomalies across the tropical Pacific Ocean.

Correspondence to: Michelle L'Heureux, Climate Prediction Center, NOAA/NWS/NCEP, 5830 University Research Court, College Park, MD 20740; E-mail: Michelle.LHeureux@noaa.gov

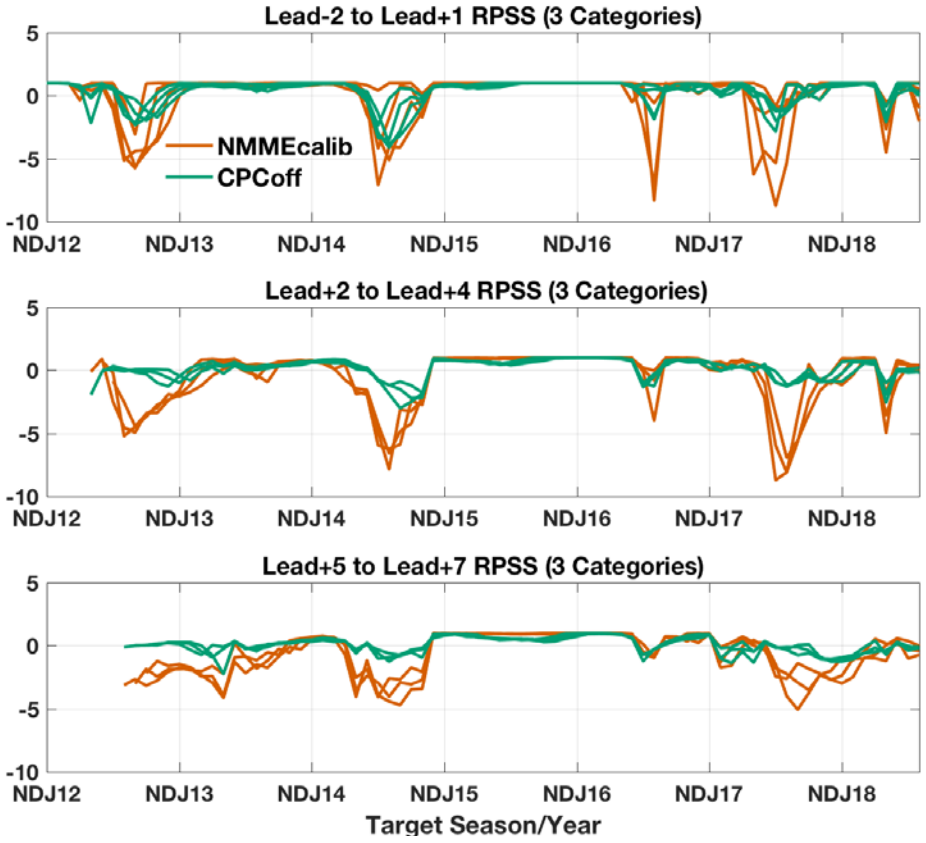

Fig. 2 The Ranked Probability Skill Score (RPSS) of the Niño-3.4 index for target seasons between November-January 2012 and July-September 2018 out to 7-months lead from the NMME (orange line) and CPC Official forecasts (green line).

Based on three-month, overlapping average values in the Niño-3.4 region, the La Niña was strongest during November 2017-January 2018 at -1.0°C relative to the 1986-2015 base period. By early May 2018, the La Niña Advisory was discontinued as the tropical Pacific Ocean returned to an ENSO-neutral state. Even while La Niña was ongoing in early 2018, many model predictions again predicted El Niño to develop during 2018. Because of the consistency of these model forecasts, even through the spring, the IRI/CPC eventually issued an El Niño Watch in early June 2018. The expectation was that El Niño would develop during the fall of 2018 and then persist into the winter 2018-19 (the NMME forecast initialized in early October 2018 is shown by the pink/purple lines in Fig. 1). However, prior to then, it was clear that the ensemble means from many dynamical models were over-predicting the level of warmth in the Niño-3.4 region for targets in the spring/summer of 2018. Instead Niño-3.4 index values were slightly positive, but shy of the +0.5°C threshold, even as the fall approached. The verification with RPSS reflects this over-prediction with a spike of negative skill in summer 2018 (Fig. 2).

2. Global temperature, precipitation, and circulation anomalies during DJF 2017-18 and their relation with ENSO

The second winter of consecutive La Niña events was accompanied by a more stereotypical La Niña pattern than the winter of 2016-17. In Fig. 4, the first La Niña is marked by the blue dot, while the second La Niña is noted with the red dot, so these two consecutive events can be directly compared. One prominent difference is that the 2017-18 winter La Niña was more strongly negative (based on Niño-3.4 index values) than the first winter, which may partially account for the more robust global footprint in the circulation and temperature (Figs. 3 and 4). In contrast to 2016-18, it is more common that the second year of La Niña is less intense than the first year, but some studies show that despite the weaker second year conditions, certain impacts can be greater (Okumura *et al.* 2017).

The left column of Fig. 3 shows observed climate anomalies during DJF 2017-18 and the right column shows the regression of these climate anomalies onto the Niño-3.4 index, which helps to diagnose the anomalies linearly associated with ENSO (note: there are also non-linear anomalies, but these are not presented herein). The regression presented in the right column are multiplied by a factor and multiplied by minus one, so that the La Niña anomalies can be seen more clearly and compared with the observations. In the top right corner of each row, the spatial correlation (with the spatial mean removed) between the observations and the ENSO

regression is displayed for 500-hPa geopotential height and winds (top row), surface temperature (middle row), and precipitation (bottom row).

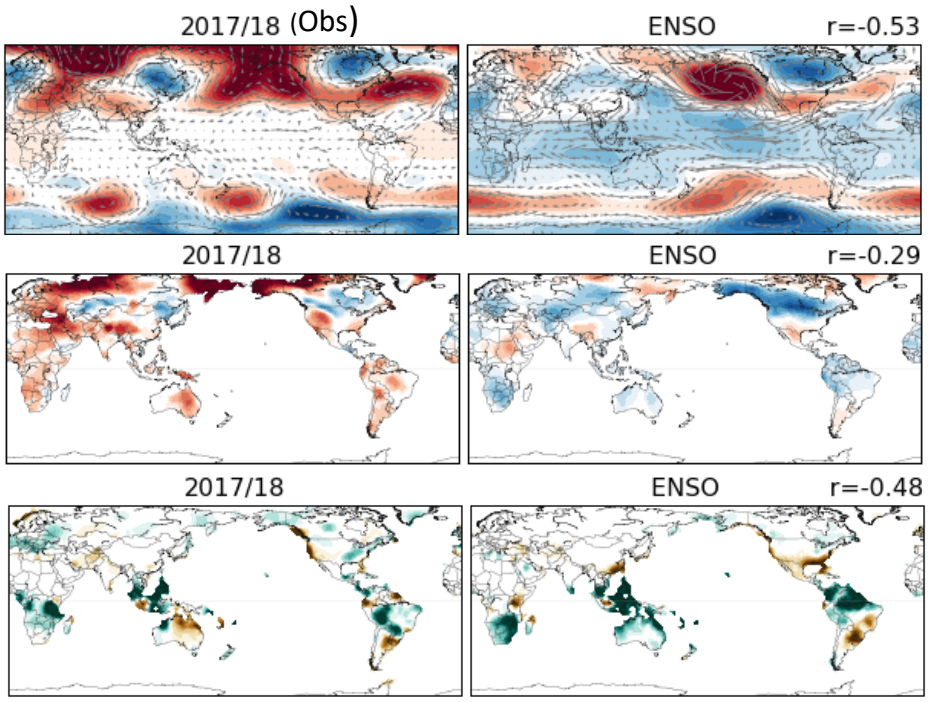

Fig. 3 December 2017-February 2018 (DJF) anomalies of 500-hPa geopotential height and winds (top row), surface temperature (middle row), and precipitation (bottom row). The left column shows the observational data, while the right column shows the reconstruction for 2017-18 (weighted regression map of the Niño-3.4 index). The reconstruction is multiplied by a factor of five to aid comparison. The r-values show the spatial correlation coefficient between the observational and the reconstructed anomalies (cosine weighted by latitude). Geopotential height and wind data is from the NCEP/NCAR Reanalysis, the temperature is from the gridded GHCN+CAMS dataset (Fan and van den Dool 2008), and precipitation data is from the gridded Precipitation Reconstruction Dataset (PREC) dataset (Chen *et al.* 2002). Departures are formed by removing monthly means during 1981-2010.

Both the circulation (top row) and precipitation (bottom) row patterns had large spatial correlations between the observations and expected linear ENSO patter (Fig. 3). The Southern Hemisphere extratropical circulation featured a positive Southern Annular Mode (or Antarctic Oscillation) pattern of above-average heights in the middle latitudes and below-average heights surrounding the South Pole. This is consistent with the expected linear relationship between ENSO and the SAM (L'Heureux and Thompson 2006). In the Northern Hemisphere, strong anomalous ridging was evident over the North Pacific Ocean, with an extension into the southern tier of the United States. Completing the expected La Niña wave train, below-average heights were observed over Canada. Also mostly consistent with La Niña, DJF 2017-18 precipitation was enhanced over the Maritime Continent, northwestern Australia, parts of southeastern Africa (excluding the southern tip), Central America, and much of Peru/Bolivia. Reduced precipitation occurred over northern Argentina and parts of the southern tier of the United States. For temperature, the observed DJF 2017-18 anomalies were considerably warmer than the expected below-average temperatures over much of the globe (Fig. 3- middle row) and, as such, the spatial correlation was reduced relative to other climate anomalies.

Figure 4 shows scatterplots between the Niño-3.4 index values and the DJF 2017-18 spatial correlations (red dot) relative to other DJF seasons between 1982 and 2018 (black dots) for 500-hPa geopotential height (left panel), surface temperature (middle panel), and precipitation (right panel). At the top of each panel in Fig. 4, the temporal correlation is provided between the Niño-3.4 index value and the spatial correlations (between the observed maps and the ENSO regression). From this analysis, it is clear that precipitation and 500-hPa heights have the strongest linkage with Niño-3.4 (r is ~0.9), meaning that larger values of Niño-3.4 are generally associated with larger spatial correlations. Phrased another way, the similarity between the observed global anomalies and the "expected" ENSO pattern is higher with stronger ENSO events. Given that DJF 2017-18 was near minus one standard deviation in Niño-3.4 index, the spatial correlations were on the stronger side. Thus, the relatively stronger event appears to have accounted for the significant La Niña features across the globe, especially in the circulation fields and precipitation patterns. In contrast, the La Niña in 2016-17 (blue

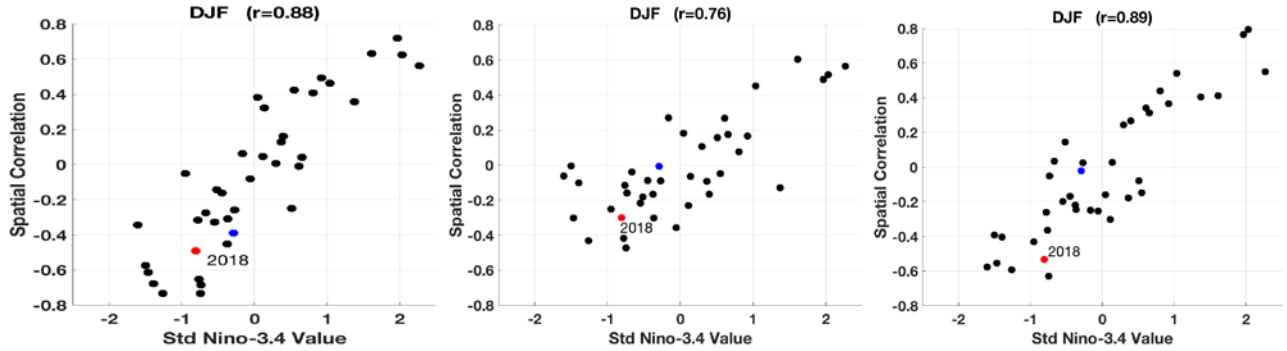

Fig. 4 Scatterplots of the spatial correlation between the ENSO regression maps of 500mb geopoential height (left panel), temperature (middle panel) and precipitation (right panel) and the observed anomalies. The spatial correlation coefficient is on the y-axis and the seasonal average Nino-3.4 index value is on the x-axis. Each dot represents a single year between 1982 and 2018. The red dot indicates the 2017-18 La Niña (the spatial correlations are also presented in Figure 3) and the blue dot indicates the 2016-17 La Niña. At the top of each panel are the temporal correlations between the Niño-3.4 values (x-axis) and the spatial correlations (y-axis). The spatial mean is removed.

dot) was only marginally so by DJF and did not have notable spatial correlations. However, both events were within the historical spread of correlations shown in these scatter plots.

Acknowledgements. The ENSO forecast team: Anthony Barnston, Emily Becker, Gerry Bell, Tom Di Liberto, Jon Gottschalck, Mike Halpert, Zeng-Zhen Hu, Nathaniel Johnson, Wanqiu Wang, Yan Xue.

References

Huang, B., P. W. Thorne, V. F. Banzon, T. Boyer, G. Chepurin, J. H. Lawrimore, M. J. Menne, T. M. Smith, R. S. Vose, and H. Zhang, 2017: Extended Reconstructed Sea Surface Temperature, Version 5 (ERSSTv5): Upgrades, validations, and intercomparisons. *J. Climate*, **30**, 8179–8205.

Chen, M., P. Xie, J. E. Janowiak, and P. A. Arkin, 2002: Global land precipitation: A 50-yr monthly analysis based on gauge observations. *J. Hydrometeor.*, **3**, 249–266.

Fan, Y. and H. van den Dool, 2008: A global monthly land surface air temperature analysis for 1948-present. *J. Geophys. Res.-Atmos.*, **113**, D01103, doi:10.1029/2007JD008470.

L'Heureux, M. L. and D. W. Thompson, 2006: Observed relationships between the El Niño–Southern Oscillation and the extratropical zonal-mean circulation. *J. Climate*, **19**, 276–287.

Reynolds, R. W., T. M. Smith, C. Liu, D. B. Chelton, K. S. Casey, and M. G. Schlax, 2007: Daily high-resolution-blended analyses for sea surface temperature. *J. Climate*, **20**, 5473–5496.

Okumura, Y. M., P. DiNezio, and C. Deser, 2017: Evolving impacts of multiyear La Niña events on atmospheric circulation and U.S. drought. *Geophys. Res. Lett.*, **44**, 11,614-11,623, doi:10.1002/2017GL075034.